Research Article

Hua Yu#, Liangliang Zhang#, Shuai Li, Fangfang Cai, Yunpeng Li, Yinkai Shi, Sujuan Zhong, Jia Ma, Yongtao Jiu, Weimin Long, Honggang Dong*, and Shizhong Wei*

Phase analysis and corrosion behavior of brazing Cu/Al dissimilar metal joint with BAl88Si filler metal

https://doi.org/10.1515/ntrev-2021-0081
received July 28, 2021; accepted August 24, 2021

Abstract: To meet the requirements of automatic production, a new type of green BAl88Si cored solder was developed. The lap brazing experiments were carried out with copper and aluminum as brazing substrates. The microstructure, phase composition, and corrosion behavior of solder joint interface were studied by field emission scanning electron microscopy, energy dispersive spectroscopy, transmission electron microscopy, electron backscattering diffraction, tensile testing machine, and electrochemical workstation. The results show that the brazing joint of Cu/BAl88Si/Al is metallurgical bonding, and the brazing joint of Cu/BAl88Si/Al is composed of Cu_9Al_4, $CuAl_2$, a-Al, ($CuAl_2$ + a-Al + Si) ternary eutectic. In addition, there is no obvious preference for each grain in the brazing joint, and there are S texture {123}<634>, Copper texture {112}<111>, and Brass texture {110}<112>. The interface of Cu_9Al_4/$CuAl_2$ is a non-coherent crystal plane and does not have good lattice matching. The average particle size of $CuAl_2$ is 11.95 μm and that of Al is 28.3 μm. However, the kernel average misorientation (KAM) value at the brazed joint interface is obviously higher than that at the brazed joint interface copper, so the defect density at the brazed joint interface aluminum is higher than that at the brazed joint interface copper. At the same time, due to poor corrosion resistance at the interface on the aluminum side of the brazed joint, serious corrosion spots and corrosion cracks occur at the same time, which leads to the shear performance of the brazed joint decreasing by about 75% after salt spray test for 240 h.

Keywords: flux filler metal, IMC, lattice mismatch, preferential orientation, KAM, corrosion behavior

1 Introduction

Copper is widely used in the manufacture of thermal components in refrigeration fields such as air conditioners and refrigerators, aerospace, and power industries because of its excellent thermal conductivity and electrical conductivity. But copper prices have long soared as resources have become increasingly scarce [1–3]. In addition, copper has a higher density, which leads to a higher quality of copper. Especially, the use of copper parts in automobiles and airplanes will improve the quality, which contradicts the concept of energy-saving and emission reduction [4,5]. Copper–aluminum composite metal joints are widely used in aerospace, air conditioning, household appliance refrigeration, and other industries and have high application value [6,7]. Aluminum and its alloys have low density, good thermal conductivity, and electrical

# These authors contributed equally to this work and should be considered first co-authors.

* **Corresponding author: Honggang Dong,** School of Materials Science and Engineering, Dalian University of Technology, Dalian, 116000, China, e-mail: donghg@dlut.edu.cn
* **Corresponding author: Shizhong Wei,** School of Material Science & Engineering, Henan University of Science and Technology, Luoyang, 471000, China; National Joint Engineering Research Center for Abrasion Control and Molding of Metal Materials, Luoyang, 471000, China, e-mail: wsz@haust.edu.cn
Hua Yu: School of Material Science & Engineering, Henan University of Science and Technology, Luoyang, 471000, China
Liangliang Zhang: School of Materials Science and Engineering, Dalian University of Technology, Dalian, 116000, China, e-mail: zll15538029120@163.com
Shuai Li: School of Mechanical Engineering, North China University of Water Resources and Electric Power, Zhengzhou 450045, China
Fangfang Cai, Yunpeng Li, Yinkai Shi: School of Material Science & Engineering, Henan University of Science and Technology, Luoyang, 471000, China; National Joint Engineering Research Center for Abrasion Control and Molding of Metal Materials, Luoyang, 471000, China
Sujuan Zhong, Jia Ma, Yongtao Jiu, Weimin Long: Zhengzhou Research Institute of Mechanical Engineering Co. Ltd., Zhengzhou, 450000, China

conductivity [8]. Therefore, in some parts, aluminum can partially or completely replace copper products, thereby greatly reducing the production costs and realizing the complementary advantages of the two metals [9,10].

The connection of Cu–Al dissimilar metals is the key technique. At present, the connection of Cu–Al dissimilar metals mainly includes mechanical connection, pressure welding, and brazing [11–13]. In the process of mechanical connection, due to the active chemical properties of aluminum, a dense oxide protective film was formed in the air. The film has a very high resistivity and is very stable under normal conditions, which seriously affects the electrical conductivity and thermal properties of the copper–aluminum connection point, resulting in premature failure of the copper–aluminum connection point [14]. In the process of press welding, the welding joint of different copper and aluminum metals with good performance can be obtained. However, there are a series of problems in pressure welding, such as high welding cost, complex process, poor adaptability to complex welding parts, long production cycle, *etc*., which restrict the application of pressure welding in different copper and aluminum welding [15,16]. However, brazing has a series of advantages such as low cost, simple equipment, and large-scale production. It has gradually become a research focus in the industry and has good development prospects. Therefore, brazing is widely used in the connection of two different metals, copper and aluminum, resulting in a joint with high strength and good airtightness [17,18]. Copper and aluminum brazing mainly use Zn–Al, Sn–Zn, and Al–Si brazing materials [19–21]. Al–Si brazing materials have good plasticity and are easy to be processed and formed. Compared with Zn–Al brazing filler metal, Al–Si brazing filler metal has better corrosion resistance, and the strength of the brazed joint is much higher than that of Sn–Zn brazing filler metal, so Al–Si brazing filler metal is more suitable for joining dissimilar metals of copper and aluminum [22,23]. However, there are few reports on the corrosion behavior of brazed Cu–Al joints with Al–Si base brazing filler metals. Huang, Ye *et al*. mainly studied the effects of Zn–Al and Sn–Zn filler metals on the corrosion microstructure and shear strength with the content of alloy element and salt spray test time [24,25].

At the same time, in the traditional brazing process, the composite application form of brazing filler metal and brazing flux usually adopts the way of placing brazing filler metal on brazing parent metal in advance or sticking brazing flux on solid brazing filler metal. This method greatly increases the pre-welding process and operation time and adds a variable during the brazing process, which affects the consistency and quality stability of welding. In addition, to ensure the quality of brazing, excessive brazing flux is often added, which will pollute the air and harm the health of operators and cause brazing flux waste [26]. Therefore, a new type of BAl88Si solder was prepared in this experiment, which meets the requirements of green manufacturing and is suitable for automatic and intelligent welding technology [27]. In addition, intermetallic compounds are the inevitable mesophase in copper–aluminum brazed joints. These hard and brittle intermetallic compounds with high resistivity will greatly reduce the performance of brazed joints and affect the integrity and stability of the joints [28,29]. However, there are few reports on the interfacial microstructure and lattice mismatch of intermetallic compounds in BAl88Si brazed Cu/Al joints.

Therefore, the lattice mismatch, texture preference orientation, and corrosion behavior of the interfacial phase in the brazed Cu–Al joint of BAl88Si were analyzed. The innovative combination of lattice mismatch and KAM value at the brazing interface and corrosion behavior at the brazing interface are helpful to study corrosion protection of copper and aluminum brazed joints in the outdoor wet environment.

2 Test materials and methods

2.1 Test material

The substrate materials used in the induction brazing experiment are copper plates and aluminum plates. The sizes of the experimental matrix materials are 70 mm × 20 mm × 2 mm and 70 mm × 30 mm × 3 mm, respectively. The chemical compositions of the basic materials and BAl88Si new solders are shown in Table 1.

2.2 Experimental method

Pretreatment of the experimental substrate before induction brazing: the substrate surface was polished with

Table 1: Chemical composition of matrix material

Materials	Cu	Al	Si	Others
T2 Copper	Base	—	—	≦0.1
1060 Aluminum	—	Base	—	≦0.4
BAl88Si	—	88	10	≦2

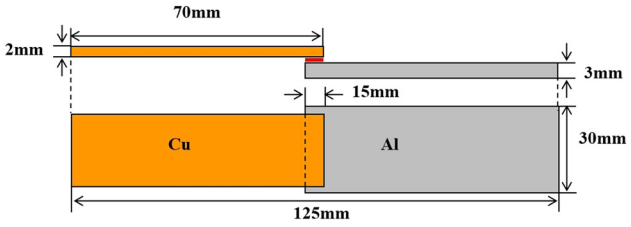

Figure 1: Model of the CU–Al brazing lap joint.

400#, 600#, and 800# sandpaper in sequence, and the polished steel plate was cleaned with alcohol ultrasonic wave. At the same time, mark a scale on the filler metal every 20 mm to quantify the filler metal during welding.

Induction brazing: the brazed joint is in the form of a lap joint, as shown in Figure 1. The lap length of the joint is 15 mm, and the substrate is fixed on the special fixture according to the lap length. Start the induction brazing machine for heating, and the current is set to 240 A. When the temperature reaches 580°C, keep the temperature for 10 s. After cooling with hollow air, the joint reaches room temperature, and the residual brazing flux and the oxide film on the surface of the substrate are removed by mechanical cleaning. The 10 mm × 10 mm joints are cut on the brazed lap joint by wire cutting, and the wire-cut joints are inlaid and polished.

After induction brazing, first, the electrochemical tests were carried out on the Cu–Al joint. The scanning speed in the experimental parameters was set to 1 mV/s, and the scanning range in the electrochemical experiment was set to ±250 mV. In the whole electrochemical experiment, the electrolyte solution composed of 3.5% sodium chloride salt and deionized water was chosen, and the solution temperature was room temperature. Second, the inlaid sample and the welded joint are put into a salt spray test box, and the sodium chloride solution with a concentration of 3.5% was poured into the saltwater tank. During the test, the temperature in the cabinet was adjusted to 35°C, and the welding samples were taken out at 0, 24, 96, 168, 240, and 480 h, respectively. Three samples were taken out at a time, rinsed with water, dried, and stored.

The morphology of the brazing joint was observed by scanning electron microscope (SEM). The composition and texture of each phase of the brazing joint were measured by energy dispersive spectrometer, electron backscatter diffraction (EBSD), and field emission scanning electron microscope. Transmission samples at the Cu/BAl88Si/Al interface were prepared by FIB technology for the first time, and the interface and phase boundary structure of the brazed joint were characterized and analyzed.

3 Results and discussion

3.1 Microstructure of the interface region of brazed joint

Figure 2 shows a scanning electron microscope image of the microstructure of the Cu/BAl88Si/Al brazing joint. Figure 2(a) shows the microstructure of brazed joints near copper. Figure 2(b) shows the micro-morphology of the middle region of the brazed joint. Figure 2(c) shows the microstructure of the brazing joint near aluminum. It can be seen from Figure 2(a) and (c) that the solder alloy has achieved good metallurgical bonding with the base metal without forming cracks or voids. Two dense intermetallic compound layers were formed at the brazing interface near Cu, with a thickness of 7–15 μm. The intermetallic compounds away from the copper interface of brazed joints tend to grow in brazed joints. In Figure 2(a)–(c), there is no obvious dense intermetallic compound at the brazing interface far from the copper side. It is composed of gray-white skeleton phase, dendritic gray-black phase, and obvious needle-like eutectic phase. Therefore, each

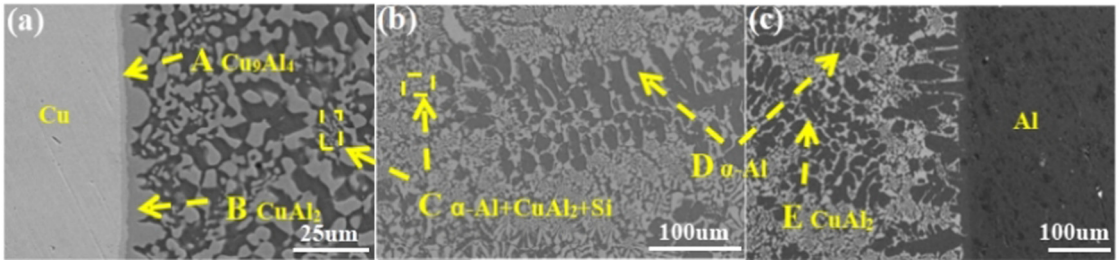

Figure 2: Scanning electron microscope image of the brazing joint of BAl88Si filler metal: (a) microstructure of the brazing joint interface on the copper side, (b) microstructure of brazing seam, and (c) microstructure of the brazed joint interface on the aluminum side.

phase in Figure 2 is subjected to energy spectrum analysis and surface analysis. The experimental results are shown in Table 1, Figures 3–5. From the surface scanning results, it can be seen that Cu elements in the base metal and brazed joint have been fully diffused, and Cu elements are mainly concentrated in the dense intermetallic compounds near the Cu side interface, as well as gray-white skeleton phase and needle-like eutectic phase in brazed joint, but the content of dendrites in the brazed joint is relatively small. At the same time, the results of surface scanning show that the total aluminum content in the gray-black phase of brazing dendrite is the highest, while the total aluminum content of needle eutectic phase, gray-white skeleton phase, and intermetallic compounds near the copper side gradually decreases. The surface scanning results showed that Si elements were obviously agglomerated in the dendrite gray-black phase and uniformly distributed in other phases of the brazing seam. The analysis results are shown in Table 2. According to the results in Table 2 and related literature, it can be inferred that the intermetallic compound formed near the interface of the copper side in Figure 2(a) is Cu_9Al_4, and the intermetallic compound beside Cu_9Al_4 is $CuAl_2$ the gray-white skeleton phase in the brazing joint is presumed to be $CuAl_2$, gray-black dendrite phase is presumed to be α-Al, and the needle-like eutectic ternary eutectic α-Al + $CuAl_2$ + Si [30]. At the brazing temperature, due to the high affinity between copper and aluminum, the molten Al–Si brazing alloy wetted the surface of the copper substrate, and the copper atoms diffused into the Al–Si brazing alloy. During the cooling process, the Cu_9Al_4 phase with high copper atom content forms on the copper/brazing interface. With a further decrease of brazing temperature, the concentration of copper atoms decreases based on Gibbs free energy, and a second IMC $CuAl_2$ phase was formed on the surface of the Cu_9Al_4 phase. In the brazing zone, Cu phase and α-Al (Cu) solid solutions are formed by diffusing copper atoms and Al–Si solder. With the decrease of temperature, the copper atoms diffused into the brazing area react with the filler metal to form ternary eutectic α-Al + $CuAl_2$ + Si [31].

3.2 Phase analysis of the interface region of brazed joint

Figure 6 shows a transmission electron microscope (TEM) image of the copper and brazing joint area. Figure 6(a) shows low-power TEM images, and Figure 6(b)–(e) shows electron diffraction patterns of different microscopic regions in Figure 6(a). There are two kinds of reaction products between copper-based metal and BAl88Si solder at the brazing interface near the copper side. According to the SAED calibration in Figure 6(c) and (d), these two intermetallic compounds are $CuAl_2$ and Cu_9Al_4, which is consistent with the results of the above energy spectrum analysis. Figure 6(b) shows the inverse fast fourier transform (IFFT) image of the interface between the $CuAl_2$ and Cu_9Al_4 metal compounds. In the fast Fourier transform corresponding to high-resolution TEM (Figure 6(e)), the (660) and (100) crystal planes of Cu_9Al_4 and the (310) and (310)

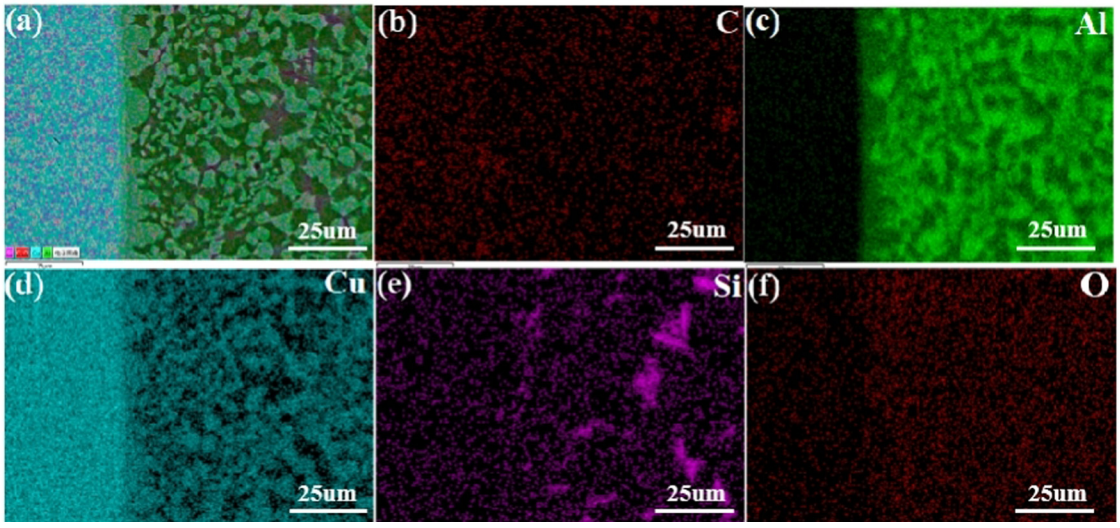

Figure 3: EDS distribution diagram of Cu side brazing joint interface: (a) surface scanning, (b) C, (c) Al, (d) Cu, (e) Si, and (f) O.

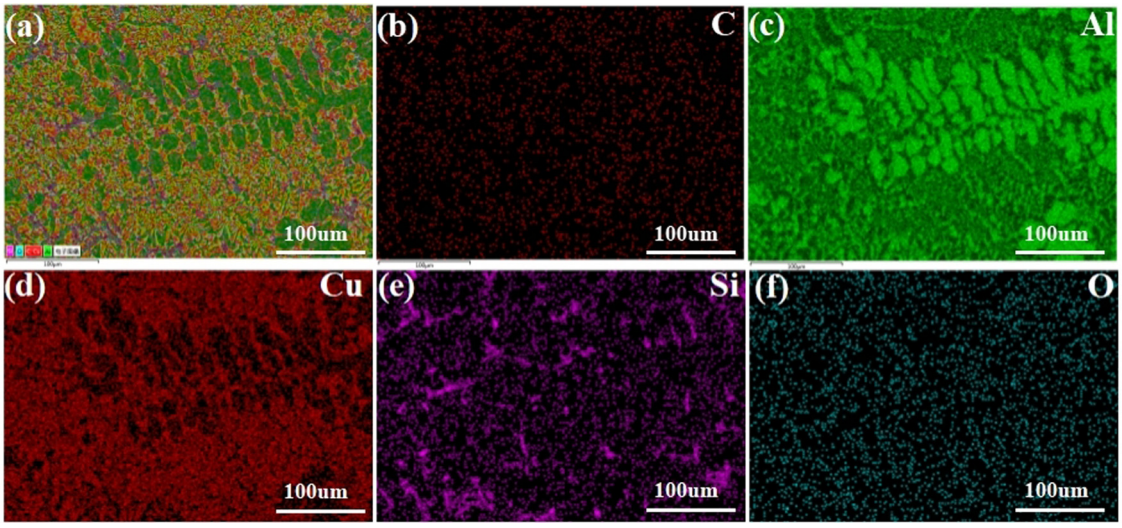

Figure 4: EDS distribution of brazing seam: (a) surface scanning, (b) C, (c) Al, (d) Cu, (e) Si, and (f) O.

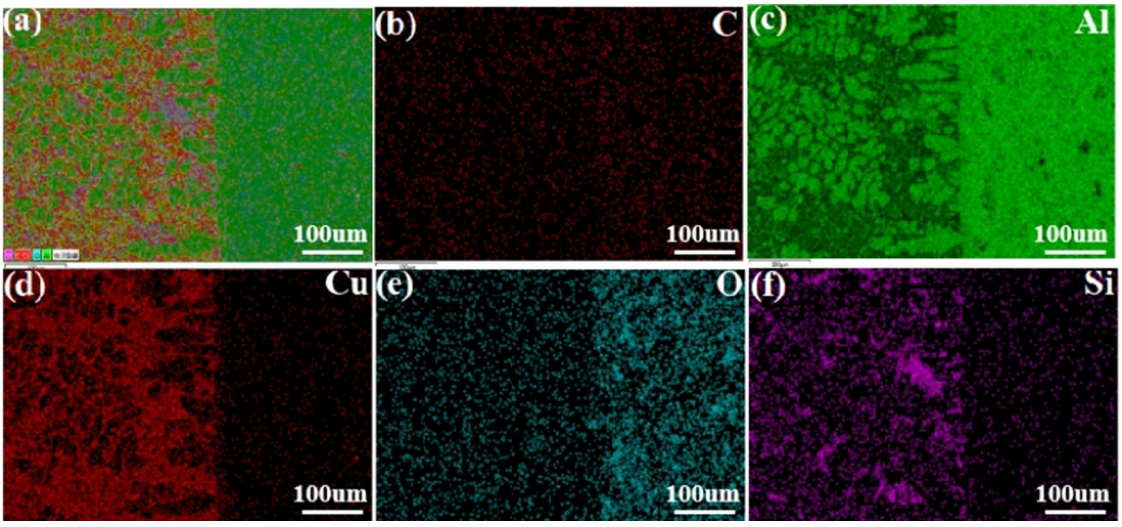

Figure 5: EDS distribution diagram of brazing seam on the CU side: (a) surface scanning, (b) C, (c) Al, (d) Cu, (e) Si, and (f) O.

Table 2: Physical phase energy spectrum of BAl88Si solder brazing joint

Measuring point	W(Al)	W(Cu)	W(Si)	W(Sb)	W(C)
a	30.16	69.84	—	—	—
b	69.76	30.24	—	—	—
c	85.2	10.68	4.12	—	—
d	98.12	—	—	—	1.88
e	68.21	29.79	—	—	2

crystal planes of Cu_9Al_4 are marked by calibrated diffraction points. The interplanar distances between the two planes are $dCuAl_2$ (310) = 1.919 nm, dCu_9Al_4 (660) = 1.025 nm, and dCu_9Al_4 (100) = 0.7944 nm. Therefore, the lattice mismatch ratio of $CuAl_2$ (310)/Cu_9Al_4 (660) crystal plane is 0.466, and the lattice mismatch ratio of $CuAl_2$ (310)/Cu_9Al_4 (100) interface is 0.586, so there is no good semi-coherent interface [32].

The crystallographic information of the interface region of the brazed joint was obtained by EBSD, and the microstructure of the interface region was further proved, as shown in Figure 7. It can be seen from Figure 7(a) that every grain in the brazed joint is anisotropic and has no obvious preferred orientation [33]. At the same time, the grain size at the copper interface of the brazed joint was significantly larger than that at the aluminum interface. Therefore, the grain size of the brazed joint was also analyzed, and the analysis results are shown in Figure 7(b), (c), and (e). Comparing the grain

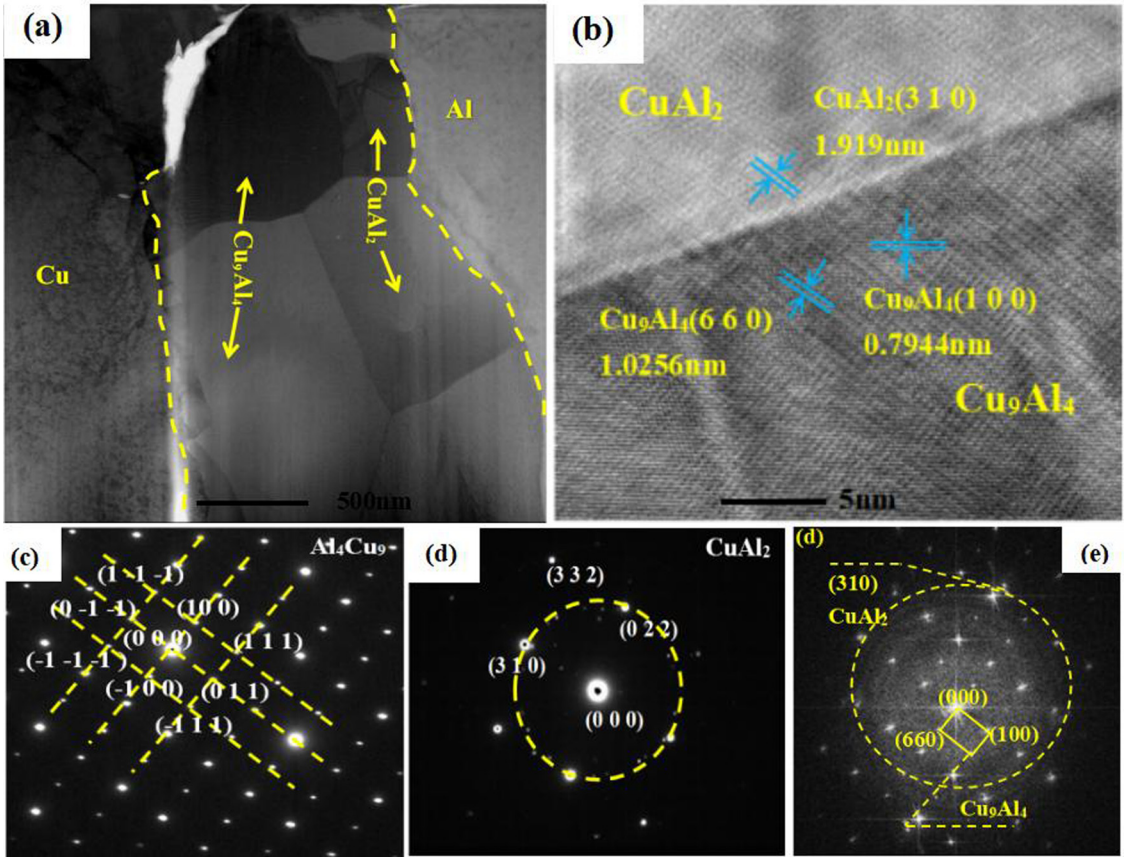

Figure 6: TEM image of interface between BAl88Si solder and Cu base metal: (a) low power TEM image of Cu and brazing joint interface, (b) $Cu_9Al_4/CuAl_2$, interface IFFT image, (c) $CuAl_2$ SAED, (d) Cu_9Al_4 SAED, and (e) $Cu_9Al_4/CuAl_2$ interface FFT.

size of the three phases, the average grain size of $CuAl_2$ is at least 11.95 μm, while the average grain size of Al is at most 28.3 μm. This is mainly due to the fact that Al grains in the molten brazing filler metal grow up continuously during the brazing process, and the heat transfer capacity of Cu is higher than that of Al, which makes the thermal energy on the fixture continuously transfer to the Cu side interface filler metal after brazing.

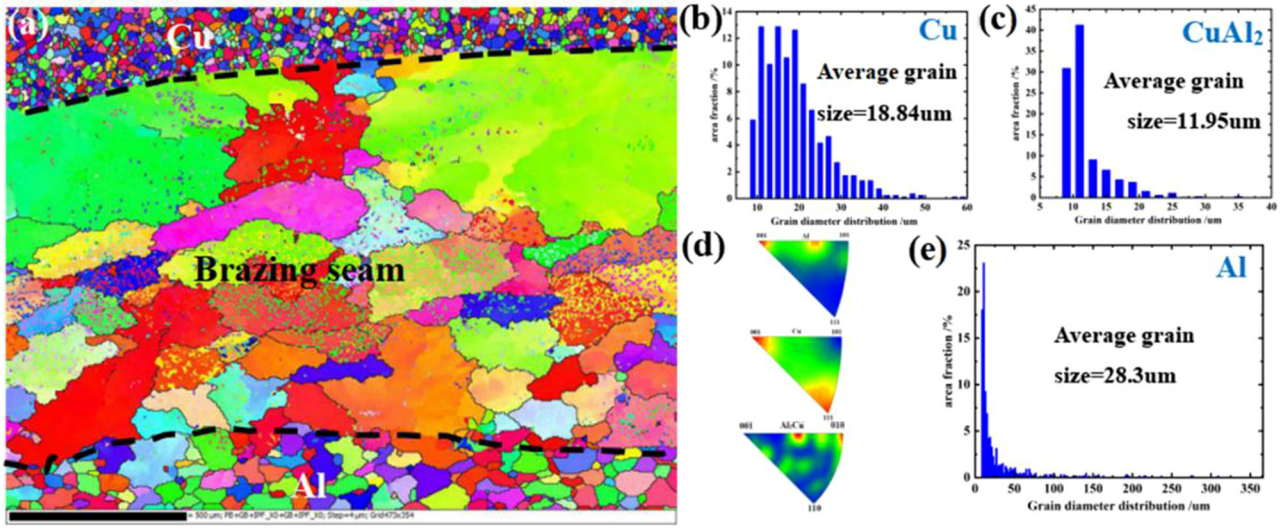

Figure 7: BAl88Si brazing joint EBSD image: (a) IPF map of the interface region, (b) grain size diagram of Cu, (c) grain size diagram of $CuAl_2$, (d) inverse polar diagram of CuAl and $CuAl_2$ and (e) grain size diagram of Al.

To further analyze the grain orientation characteristics of Cu, Al, and $CuAl_2$, by processing EBSD data, the polar diagram of each phase is obtained, as shown in Figure 8. Compared with the standard texture, there are S texture {123}<634>, Copper texture {112}<111>, and Brass texture {110}<112> in the brazing joint [34].

Figure 9(a) shows the KAM diagram corresponding to the inverted diagram of Figure 9(d), from which the distortion density and distribution at the interface of brazing joints can be explained. It can be seen from the figure that the KAM value on the brazed joint aluminum interface is obviously higher than that at the brazed joint copper interface, which means that defect density on the brazed joint aluminum interface is higher than that on the brazed joint copper interface [35]. Figure 9(b) shows the distribution of grain boundaries in the brazed joint. It can be seen that there is a grain boundary with a large angle at the interface of brazing joint Al, which means that the grain size at the interface of brazing joint Al is smaller and more uniform than that at the Cu interface. Figure 9(c) is the recrystallization diagram of the brazed connection. It can be seen that the KAM value at the brazing joint Cu side interface is lower than the KAM value at the brazing joint aluminum side interface, so the grain boundary migration rate at the aluminum side interface is higher than that at the Cu side interface in the recrystallization process [36].

3.3 Corrosion behaviors of brazed joints

Figure 10 is the electrochemical test chart of brazing, copper, and aluminum, wherein Figure 10(a) is a Tafel curve. Figure 10(b) is the impedance curve and Figure 10(c) is the electrochemical sample graph. By comparing figures, it can be found from Figure 10(a) and (b) that the maximum corrosion potential of copper is −0.096 V and the impedance radius is the smallest. However, Al and brazing seam corrosion potential are both lower than Cu, which are −0.831 and −0.757 V, respectively, and the impedance radius is larger. And the corrosion current density of the brazed joint is 8.456×10^5. Therefore, when the copper-aluminum joint is placed in the salt spray test chamber, the corrosion resistance of the copper side interface of the brazed joint is significantly higher than that of the aluminum side interface of the brazed joint [37].

After the neutral salt spray test for 480 h, the microscopic corrosion morphology and shear performance of the brazed joint in each period are shown in Figure 11. Figure 11(a) shows the microscopic corrosion morphology of the brazed joint at 480 h; it can be clearly seen that pitting pits with a depth of 140–170 μm are formed at the aluminum interface of the brazed joints, which is consistent with the conclusion that the corrosion resistance of the aluminum interface is low. Figure 11(b) shows the

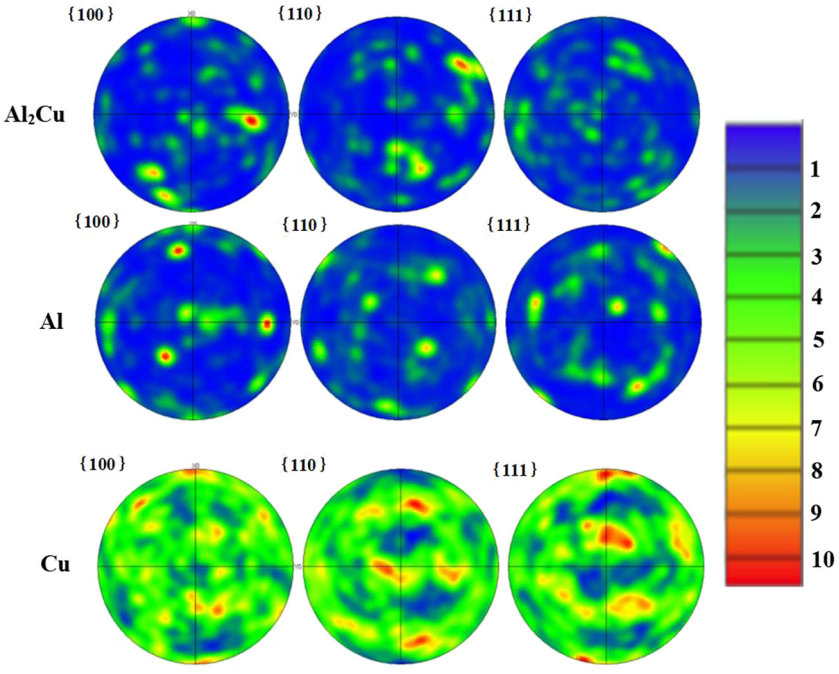

Figure 8: Pole figures of Cu, Al, and Al_2Cu in the BAl88Si brazing point.

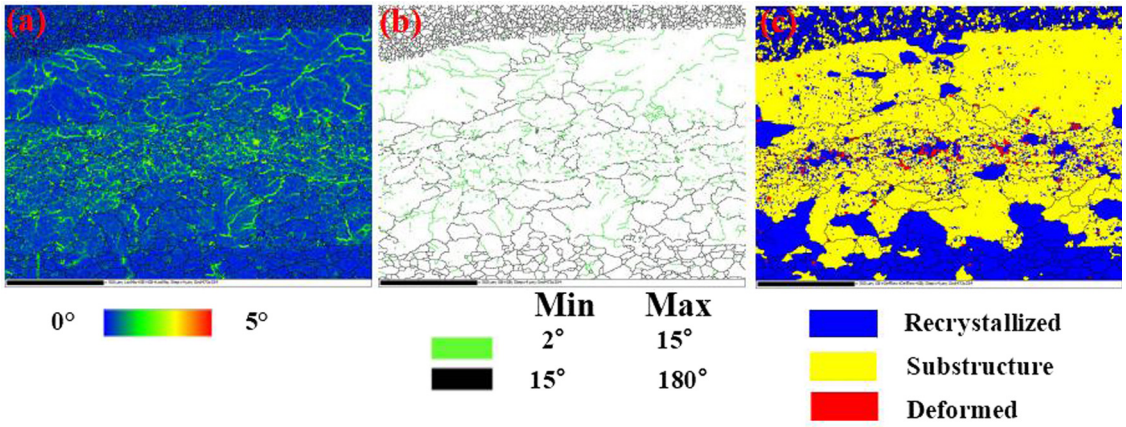

Figure 9: (a) KAM diagram, (b) grain boundary diagram, and (c) recrystallation diagram of brazing joints.

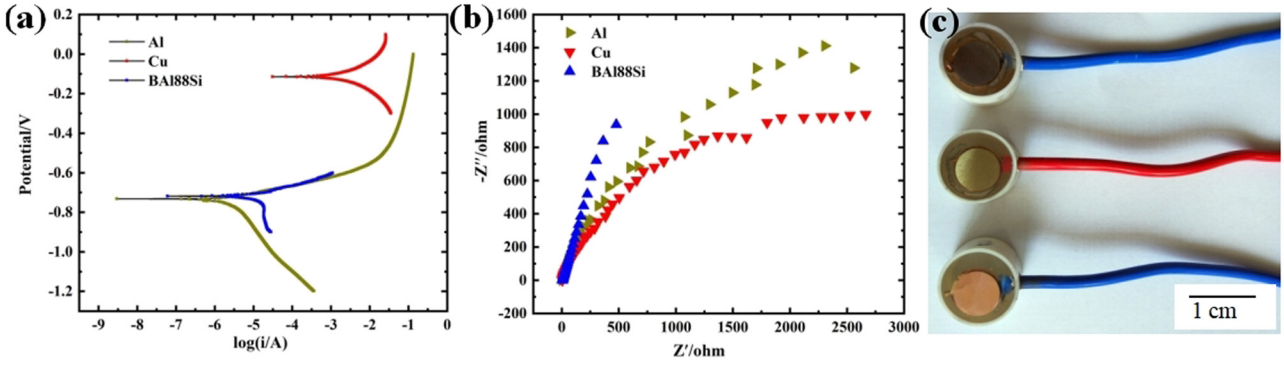

Figure 10: Image of electrochemical results: (a) Tafel polarization curves of the solder and base metal; (b) electrochemical impedance spectroscopy of the solder and base metal, and (c) diagram of samples for electrochemical tests.

corrosion crack morphology after 96 h of salt spray corrosion, and Figure 11(c) is an enlarged view of Figure 11(b). It can be clearly observed that cracks have been formed at the interface between the aluminum side and the brazed joint, and the corrosion crack continues to spread with a-Al. During the shear test, the stress corrosion crack tip of the diffusion layer becomes the stress concentration point, which will seriously reduce the mechanical properties of the joint [38]. This is because the radius of Cl^- in the salt spray test is very small, so it can be adsorbed on the surface of the sample and combined with cations in the metal on the surface of the sample to form soluble chloride and then become pitting corrosion nuclei [39]. In this way, the pitting core can corrode the surface of the substrate, and the pitting core will continue to grow, which will lead to the dissolution of the metal anode and gradually becoming pitting pits. This is how the pits observed in Figure 11(a) are generated. The neutral salt spray corrosion is electrochemical corrosion, in which metal is the anode and the other areas are the cathode, thus forming a corrosion cell.

Reduction reaction takes place in the cathode:

$$O_2 + 2H_2O + 4e^- \rightarrow 4OH^-.$$

Aluminum is oxidized at the anode:

$$Al \rightarrow Al^{2+} + 2e^-.$$

As the progress of redox reaction, the anions generated by the cathode attract the cations to move to the cathode, while the actions generated by the anode attract Cl^- to move to the anode, and the corrosion continues. With the decrease of pH value in local corrosion pits, pitting corrosion expands and deepens, and the number and area of small pitting corrosion pits increase and gradually expand to the surrounding area and develop into comprehensive corrosion [40].

It can be seen from Figure 11d. The shear strength of the joint before the salt spray test was 64 MPa. With the increase of salt spray corrosion time, the overall shear strength of the sample decreased significantly. The tensile strength decreased by nearly 50% at 96 h, and by nearly 75% at 240 h. In the first 240 h, the tensile strength of the sample decreased obviously, which was mainly

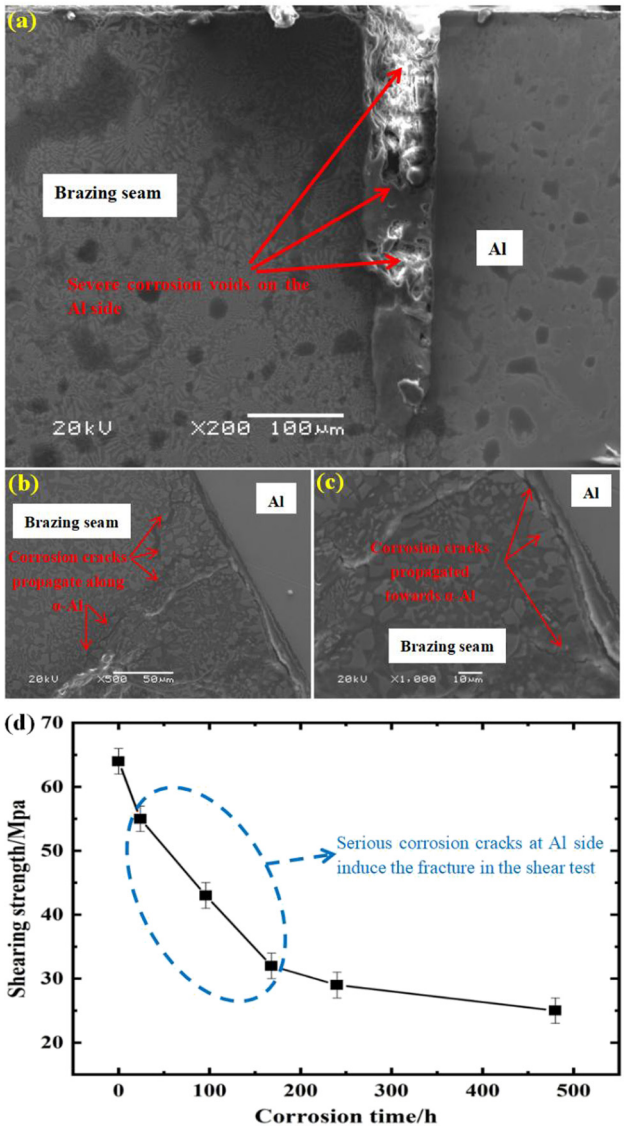

Figure 11: (a) Typical microstructure of brazing seam after salt spray test, (b) microstructure of corrosion crack propagation in the Brazed joint, (c) enlarged image of (b), and (d) shearing strength of joints brazed after salt spray tests.

due to the corrosion crack at the Al side interface of the brazed joint, which reduced the mechanical properties of the joint to the greatest extent, which was consistent with the microstructure analysis mentioned above.

4 Conclusion

The experimental results show that the copper–aluminum joint brazed with new green BAl88Si brazing filler metal can obtain good metallurgical bonding as a whole, and no cracks and voids are formed. The interface at the brazed Cu side is composed of two layers of dense intermetallic compounds with a thickness of 7–15 μm, Cu_9Al_4 and $CuAl_2$. The lattice mismatch rate of the crystal surface of $CuAl_2$ (310)/Cu_9Al_4 (660) and the interface of $CuAl_2$ (310)/Cu_9Al_4 (100) is 0.466 and 0.586, respectively. Therefore, there is no good semi-coherent interface between these two intermetallic compounds. The interface away from brazing copper is mainly composed of gray skeleton phase $CuAl_2$, dendrite gray-black phase a-Al, and obvious needle eutectic phase ternary eutectic a-Al + $CuAl_2$ + Si. The mean grain size of $CuAl_2$ in the brazed joint is 11.95 μm, while that of Al was 28.3 μm. However, the KAM value of the brazed joint aluminum interface is obviously higher than that of the brazed joint copper interface, so the defect density of the brazed joint aluminum interface is higher than that of the brazed joint copper interface. At the same time, due to poor corrosion resistance at the aluminum interface of the brazed joint, serious pitting corrosion and corrosion cracks appeared, resulting in the shear performance of the brazed joint decreased by nearly 75% in the first 240 h.

Acknowlegment: The authors gratefully acknowledge funding from the Key Projects of Strategic International Scientific and Technological Innovation Cooperation (grant no. 2016YFE0201300); project (SKLABFMT201902) supported by the State Key Laboratory of Advanced Brazing Filler Metals and Technology, Zhengzhou Research Institute of Mechanical Engineering, Zhengzhou, China; project (20A430013) supported by the Education Department of Henan Province, China.

Funding information: Key Projects of Strategic International Scientific and Technological Innovation Cooperation (grant no. 2016YFE0201300); project (SKLABFMT201902) supported by the State Key Laboratory of Advanced Brazing Filler Metals and Technology, Zhengzhou Research Institute of Mechanical Engineering, Zhengzhou, China; project (20A430013) supported by the Education Department of Henan Province, China.

Author contributions: All authors have accepted responsibility for the entire content of this manuscript and approved its submission.

Conflict of interest: The authors state no conflict of interest.

References

[1] Wang XG, Li XG, Yan FJ, Wang CG. Effect of heat treatment on the interfacial microstructure and properties of Cu–Al joints. Weld World. 2016;61(1):1–10.

[2] Krishna BV, Venugopal P, Rao KP. Effect of heat treatment and interlayer on weld strength and microstructure of solid state joints between Cu and Al powder metallurgical preform tubes. Sci Technol Weld Join. 2005;10(3):259–67.
[3] Wan JB, Liu YC, Wei C, Jiang P, Gao ZM. Effect of the soldering time on the formation of interfacial structure between Sn–Ag–Zn lead-free solder and Cu substrate. J Mater Sci Mater Electron. 2008;19(12):1160–8.
[4] Lee WB, Bang KS, Jung SB. Effects of intermetallic compound on the electrical and mechanical properties of friction welded Cu/Al bimetallic joints during annealing. J Alloy Compd. 2005;390(1–2):0–219.
[5] Xia CZ, Li YJ, Puchkov UA, Gerasimov SA, Wang J. Crack analysis near vacuum brazing interface of Cu/Al dissimilar materials using Al–Si brazing alloy. Mater Sci Technol. 2009;25(3):383–7.
[6] Shinozaki K, Koyama K. Development of Al/Cu dissimilar brazing joint controlled form of intermetallic compound. Mater Sci Forum. 2007;539:4075–80.
[7] Wang XG, Yan FJ, Li XG, Wang CG. Induction diffusion brazing of copper to aluminium. Sci Technol Weld Join. 2017;22(2):170–5.
[8] Feng JC, He P. High frequency induction contact reactive brazing of aluminum to stainless steel. Trans Nonferrous Met Soc China. 2005;15(S2):11–5.
[9] Mao Z, Xie J, Wang A, Wang W, Li Y, Ma D. Interfacial microstructure and bonding strength of copper/aluminum clad sheets produced by horizontal twin-roll casting and annealing. Mater Res Express. 2018;6(1):016505.
[10] Yang M, Peng H, Lin T. Effect of brazing conditions on microstructure and mechanical properties of Al2O3/Ti—6Al—4V alloy joints reinforced by TiB whiskers. J Mater Sci & Technol. 2013;29(10):961–70.
[11] Zhang L, Yu H, Ma J, Zhong S, Jiu Y, Wei S, et al. Microproperties and interface behavior of the BAg25TS brazed joint. Vacuum. 2019;169:108928.
[12] Kim HG, Kim SM, Lee JY, Choi MR, Choe SH, Kim KH, et al. Microstructural evaluation of interfacial intermetallic compounds in Cu wire bonding with Al and Au pads. Acta Materialia. 2014;64:356–66.
[13] Pouranvari M, Abbasi M. Dissimilar gas tungsten arc weld-brazing of Al/steel using Al–Si filler metal: microstructure and strengthening mechanisms. J Alloy Compd. 2018;749:S0925838818310946.
[14] Lee EJ, Patel A, Acedillo RR, Bachynski JC, Barrett I, Basile E, et al. Research on the corrosion resistance of Cu–Al joints brazed with flux-cored Zn-2Al filler metal. Mater Res Express. 2019;6(5):2053.
[15] Xia CZ, Li YJ, Wang J, Ma HJ. Microstructure and phase constitution near interface of Cu/Al vacuum brazing. Mater Sci Technol. 2007;23(7):815–8.
[16] Xia C, Li Y, Puchkov UA, Gerasimov SA, Wang J. Microstructure and phase constitution near the interface of Cu/Al vacuum brazing using Al–Si filler metal. Vacuum. 2008;82(8):799–804.
[17] Yan F, Xu D, Wu SC, Sun Q, Wang C, Wang Y. Microstructure and phase constitution near the interface of Cu/3003 torch brazing using Al–Si–La–Sr filler. J Mech Sci Technol. 2012;26(12):4089–96.
[18] Ghasemi S, Shanaghi A, Chu PK. Nano mechanical and wear properties of multi-layer Ti/TiN coatings deposited on Al 7075 by high-vacuum magnetron sputtering. Thin Solid Films. 2017;638:96–104.
[19] Palit D, Meier AM. Reaction kinetics and mechanical properties in the reactive brazing of copper to aluminum nitride. J Mater Sci. 2006;41(21):7197–209.
[20] Peng D, Kaihua C, Rongshi X. Mechanical properties of aluminum-copper joint by laser penetration brazing. Chin J Lasers. 2011;38(6):0603009.
[21] Long WM, Lu QB, He P, Xue SB, Wu MF, Xue P. In situ synthesis of Al–Si–Cu alloy during brazing process and mechanical property of brazing joint. J Mater Eng. 2016;44(6):17–23.
[22] Kim IK, Hong SI. Effect of heat treatment on the bending behavior of tri-layered Cu/Al/Cu composite plates. Mater Des. 2013;47:590–8.
[23] Pugal D, Kim KJ, Aabloo A. An explicit physics-based model of ionic polymer-metal composite actuators. J Appl Phys. 2011;110(8):084904.
[24] Huang S, Long WM, Lu QB, Jiu YT, Zhong SJ. Research on the corrosion resistance of Cu-Al joints brazed with flux-cored Zn-2Al filler metal. Mater Res Express. 2019;6–5.
[25] Ye Z, Yang H, Huang J, Yang J, Chen S. A novel Zn-Al-Si corrosion resistant filler metal for Cu/Al brazing. Mater Lett. 2017;206:(nov. 1):201–4.
[26] Xu C, Lang Q, Wang Q, Chen Y, Yan J, Chen S. Microstructure and mechanical properties of ultrasound-assisted soldered Al-50 wt%Si/Al-27 wt%Si joints for automotive applications. JOM. 2019;71(6):2025–32.
[27] Jl F, Xue S, Lou J, Lou Y, Wang S. Microstructure and properties of Cu/Al joints brazed with Zn–Al filler metals. Trans Nonferrous Met Soc China. 2012;22(2):281–7.
[28] Feng J, Songbai X, Wei D. Reliability studies of Cu/Al joints brazed with Zn–Al–Ce filler metals. Mater Des. 2012;42:156–63.
[29] Tang J, Zhang L, Zhou T, Sun Z, Kong L, Jing L, et al. Growth characterization of intermetallic compounds at the Cu/Al solid state interface. Mater Res Express. 2019;6(10):106544.
[30] Yu H, Zhang L, Cai F, Zhong S, Ma J, Bao L, et al. Microstructure and mechanical properties of brazing joint of silver-based composite filler metal. Nanotechnol Rev. 2020;9:1034–43.
[31] Pei Y, Huang T, Chen F, Pang B, Guo J, Xiang N, et al. Microstructure and fracture mechanism of Ti/Al layered composite fabricated by explosive welding. Vacuum. 2020;181:109596.
[32] Hsu HC, Chien JH, Chu LM, Ju SP, Feng YT, Fu SL. Nanoscale bondability study on copper-aluminum intermetallic compound using molecular dynamics simulation. Microsystems, Packaging, Assembly & Circuits Technology Conference. IEEE; 2013.
[33] Battiston E, Salvatici MC, Lavacchi A, Gatti A, Di Marco S, Mugnai L. Functionalization of a nanostructured hydroxyapatite with copper(II) compounds as pesticide: in situ TEM and ESEM observations of treated Vitis vinifera L. leaves. Pest Manag Sci. 2018;74(8):1903–15.
[34] Ali ZI, Ghazy OA, Meligi G, Saleh HH, Bekhit M. Copper nanoparticles: synthesis, characterization and its application as

catalyst for p-Nitrophenol reduction. J Inorg Organomet Polym Mater. 2018;8:1–11.
[35] Wei Y, Sun F, Tan S, Liang S. Study on microstructure and performance of transient liquid phase bonding of Cu/Al with Al-based interlayers. Vacuum. 2018;154:18–24.
[36] Yan MF, Zhu YD, Zhang YX, Zhang ML. Combining thermo-diffusing titanium and plasma nitriding to modify C61900 Cu–Al alloy. Vacuum. 2016;126:41–4.
[37] Tang J, Zhang L, Zhou T, Sun Z, Kong L, Jing L, et al. Growth characterization of intermetallic compounds at the Cu/Al solid state interface. Mater Res Express. 2019;6(10):407–18.
[38] Xu B, Tong WP, Liu CZ, Zhang H, Zuo L, He JC. Effect of high magnetic field on growth behavior of compound layers during reactive diffusion between solid Cu and liquid Al. J Mater Sci Technol. 2011;9:90–4.
[39] Gueydan A, Domengès B, Hug E. Study of the intermetallic growth in copper-clad aluminum wires after thermal aging. Intermetallics. 2014;50:34–42.
[40] Yu H, Zhang L, Cai F, Zhong S, Ma J, Zhang Y, et al. Interface microstructure and growth mechanism of brazing Cu/Al joint with BAl88Si filler metal. Vacuum. 2020;181:109641.